Available online at www.sciencedirect.com

ScienceDirect

Comput. Methods Appl. Mech. Engrg. 275 (2014) 39–54

Computer methods in applied mechanics and engineering

www.elsevier.com/locate/cma

In-plane mesh regularization for node-based shape optimization problems

Electra Stavropoulou *, Majid Hojjat, Kai-Uwe Bletzinger

Lehrstuhl für Statik, Technische Universität München, Arcisstr. 21, 80333 München, Germany

Received 10 December 2012; received in revised form 1 February 2014; accepted 22 February 2014
Available online 5 March 2014

Abstract

In this contribution a global and linear method for controlling the surface mesh quality during node-based shape optimization is presented. In this method, an artificial stress is applied on the surface mesh and the global linear system of equations is solved for the equilibrium state by finite elements. The applied stress adapts each element towards a desired predefined template geometry and at the end a globally smooth mesh is achieved. In this way both the shape and the size of each element is controlled. Some examples, as well as possible fields of application are shown. At the end, the strength of the method in shape optimization of computational fluid dynamics problems is described.

Keywords: Aerodynamic shape optimization; Node-based; CAD-free; Mesh smoothing; In-plane regularization

1. Introduction

Optimal shape design receives great attention in aerospace, marine and automotive industry where the aim is to minimize a functional that describes mechanical characteristics of the design. A key element in this process is the definition of the parametrization of the shape. Inspired from engineering design, Computer Aided Geometric Design (CAGD) methods have been commonly used to represent the shape for both structure and fluid problems. In this instance, the design parameters of the CAD are the design variables of the optimization problem. The limited number of design variables allows efficient computation of direct sensitivities. In contrary, the low number of design variables restricts the design space not being able to produce all the shape modes needed to capture the optimum.

Adjoint methods provide sensitivity values on every discretization element (cell, point, etc.) almost by the same cost as the primal problem [1,2]. This motivates the use of enriched design spaces with larger number of

* Corresponding author. Tel.: +49 89 289 22152; fax: +49 89 289 22421.
E-mail addresses: stavropoulou@tum.de (E. Stavropoulou), hojjat@tum.de (M. Hojjat), kub@tum.de (K.-U. Bletzinger).

http://dx.doi.org/10.1016/j.cma.2014.02.013
0045-7825/

design variables. In contrast to CAD methods, the node-based shape optimization approach regards the design space to be as large as possible by considering directly the node positions as design variables. Hence, the discretization of the design surface is also used to describe the geometry and provides the vertex coordinates as design variables for the optimization problem.

This method suffers from mesh dependent results and non-smooth derivatives which almost always lead to unphysical and jagged shapes [3]. For this reason various projection methods are suggested which smoothen the variation of the shape in the "out of plane" direction [4–7]. However, updating the discrete surface only in the normal direction without regarding any changes in the tangent to the surface direction can lead to high distortion of the surface elements [5,8,9]. As a result, an "in-plane" regularization step is also required to ensure the quality of the surface discretization during optimization.

Generally, in the field of mesh quality control there are two main classes of problems: the mesh quality improvement and the mesh motion problems. In mesh smoothing, the goal is to improve the quality of a 2D or 3D mesh [10–13] whereas in mesh motion problems the resulting 2D or 3D mesh is seeked after moving a 1D or a 2D boundary respectively [14–16]. In both fields the ideas are similar. As the mesh motion solvers advance, bigger boundary updates can take place. These larger modifications of the design surface give rise to the mesh distortion problem of the boundary. For this reason, in-plane regularization methods are required which deal with retaining the surface mesh quality during the evolution of the shape [5,8].

Within this contribution, a global method which regularizes the surface mesh to a desired condition is presented. In this method, an artificial stress field is applied on the surface or on the volume mesh and a global linear system for the equilibrium is solved. The applied stress adapts the shape of each element towards a desired predefined template geometry and at the end a globally smooth mesh is achieved. In this way, both shape and size of each element is controlled. The method can be applied on both structured and unstructured grids since there is no additional assumption on the mesh topology.

The remainder of this article is organized as follows: Section 2 introduces the shape optimization problem and the in-plane regularization term of the augmented problem. In Section 3, a short overview is given on the methods used so far for mesh smoothing and mesh quality control. The proposed in-plane regularization method is discussed in Section 4 and in the next section, the role of the fundamental components of the method is demonstrated. Finally, numerical results of minimization of power loss in a ducted flow and conclusions are presented in sections 6 and 7, respectively.

2. The optimization problem

In general, in node-based shape optimization the shape is described only by the discretization and no other geometrical link is established. Therefore, the coordinates of the surface nodes are considered to be the design variables of the optimization problem, since changing the position of the internal nodes will not alter the shape. More precisely, the position of the surface point can be decomposed into two components, normal and tangential to the surface, as follows:

$$\boldsymbol{x}_l = x_{l,n} \cdot \boldsymbol{n} + x_{l,t} \cdot \boldsymbol{t} = s_l \cdot \boldsymbol{n} + r_l \cdot \boldsymbol{t}, \quad l = 1, \ldots, n_s. \tag{1}$$

n_s is the number of surface nodes and $\boldsymbol{n}$ and $\boldsymbol{t}$ are the unit vectors normal and tangential to the surface at node l.

Neglecting the discretization error and the finite step size of the optimization, small variations of $x_{l,n}$ in the "out of plane" direction will cause a change in the shape, while small variation of $x_{l,t}$ in the "in-plane" direction will only alter the discretization. In other words, $x_{l,n}$ is the shape relevant component s_l, while $x_{l,t}$ is the mesh relevant component r_l. For this reason only the normal component s_l is regarded as design variable and consequently in each optimization step only the out of plane direction is updated. However, during this process the quality of elements could deteriorate and severely distorted elements might appear. In extreme cases, the elements become degenerate and further progress of analysis is restricted. Hence, a correction in the "in-plane" direction is required.

For this reason, the optimization problem with response function f, constraints (g_j, h_k) and variable bounds $(s_l^{lower}, s_l^{upper})$ for each surface node l is modified as follows:

$$\begin{aligned} & \tilde{f}(\boldsymbol{s},\boldsymbol{r}) = f(\boldsymbol{s},\boldsymbol{r}) + R(\boldsymbol{s},\boldsymbol{r}) \rightarrow min, \\ s.t. \quad & g_j = g_j(\boldsymbol{s},\boldsymbol{r}) \leqslant 0, \quad j \in 1,\ldots,N_j, \\ & h_k = h_k(\boldsymbol{s},\boldsymbol{r}) = 0, \quad \forall k \in 1,\ldots,N_k, \\ & s_l^{lower} \leqslant s_l \leqslant s_l^{upper}, \quad \forall s_l \in \mathbb{R}, l = 1,\ldots,n_s. \end{aligned} \tag{2}$$

$\tilde{f}$ is the augmented objective function of the original objective f modified by a regularization term R responsible for retaining the mesh quality. The surface sensitivity of the augmented objective function $\tilde{f}$ is:

$$\frac{d\tilde{f}}{d\boldsymbol{s}} = \frac{df}{d\boldsymbol{s}} + \frac{dR}{d\boldsymbol{s}}. \tag{3}$$

The augmented objective function should not alter the problem and since the only shape modifications occur in the normal to the surface direction, the term R should be modeled such that the shape derivative of the modified optimization problem is the same as the initial one, i.e.:

$$\frac{d\tilde{f}}{d\boldsymbol{s}} = \frac{df}{d\boldsymbol{s}}. \tag{4}$$

Here, in order to prevent any influence from the mesh regularization term on the original optimization problem, we define R such that its derivative with respect to the normal direction is zero. Also, in absence of discretization errors it holds in the tangent space:

$$\frac{df}{d\boldsymbol{r}} = 0 \quad \text{and} \quad \frac{d\tilde{f}}{d\boldsymbol{r}} = \frac{dR}{d\boldsymbol{r}}. \tag{5}$$

Of course after discretization, the effects of $\boldsymbol{s}$ and $\boldsymbol{r}$ are not as clearly separated anymore and discretization errors have to be accepted. Still the regularization term R controls the mesh quality. This term and its modeling is the main focus of this paper.

3. Overview of elliptic mesh quality control methods

Generally, various methods have been developed for mesh smoothing (mesh relaxation) and mesh deformation. The ideas in these two fields are often similar. The proposed methods for this type of problems can be geometrically, mechanically or mathematically motivated and the vast majority apply elliptic equations either for smoothing the mesh or for propagating the motion of a boundary to the domain. Among the elliptic mesh generators, the Amsden–Hirt and the Thompson–Thames–Mastin grid generators are broadly used [10,17] for both structured and unstructured grids. Variations of the same operators apply also to mesh motion problems [16,14].

In the Amsden–Hirt method, the transformation between a square logical domain and the physical surface which needs to be discretized is sought. This transformation is considered to satisfy the following variational form:

$$I_{AH} = \frac{1}{2}\int\int_0^1 (\boldsymbol{g}_1 \cdot \boldsymbol{g}_1 + \boldsymbol{g}_2 \cdot \boldsymbol{g}_2) dA \rightarrow \min_r, \tag{6}$$

where $\boldsymbol{g}_1$ and $\boldsymbol{g}_2$ are the covariant base vectors of the physical domain and the integration is performed over the square logical domain. Minimization of this functional will lead to the Laplace equation of the transformation map from the logical to the physical domain. By solving this variational problem, the resulting transformation may have zero Jacobian and non-folded meshes in non-convex domains are not guaranteed [11]. Solved in a local manner the equation reduces to the well know Laplacian smoother.

The Thompson–Thames–Mastin method guaranties non-zero Jacobians for the continuum problem by solving the same Laplacian problem for the inverse of the aforementioned transformation. Thus, the functional describing the method is the following:

$$I_{TTM} = \int_\Omega (\boldsymbol{g}^1 \cdot \boldsymbol{g}^1 + \boldsymbol{g}^2 \cdot \boldsymbol{g}^2) d\alpha \rightarrow \min_r, \tag{7}$$

where $\boldsymbol{g}^1$ and $\boldsymbol{g}^2$ are the contravariant base vectors of the physical domain and the integration is performed over the physical space. Unlike the Amsden–Hirt method, this equation leads to a nonlinear system of equations. Hansen et al. in [18] extended this method for mesh smoothing of unstructured meshes by discretizing the resulting equation with finite elements and using a metric which incorporates influences from the neighboring elements.

The regularization method presented in the next section is also an elliptic method and is mechanically motivated. It will be shown that in special cases, it reduces to the Amsden–Hirt method.

4. The regularization method

The proposed mesh regularization method is inspired by form-finding which is a method to determine the free-form equilibrium shape of membrane and shell structures subjected to a certain stress field [19–21]. In other words, assuming a stress field applied on the resulting structure, the displacement field which brings the system to equilibrium is seeked. Consequently, since no body forces and surface traction are regarded, the weak form of equilibrium in the context of geometrical nonlinear analysis reduces to the internal virtual work done by the predefined stress field:

$$\delta w(\boldsymbol{s},\boldsymbol{r}) = \delta w_{int} = t\int_a \boldsymbol{\sigma}_0 : \delta\boldsymbol{\epsilon} da = 0. \tag{8}$$

$\boldsymbol{\sigma}_0$ is the prescribed Cauchy stress tensor components acting on the resulting geometry with area a and $\boldsymbol{\epsilon}$ the Euler–Almansi strain tensor [22]. The membrane stresses are considered constant through the thickness t. Therefore, the integration is performed on the mid-surface of the structure. When constant isotropic stress field is applied, the resulting surface is a minimal surface, which is the surface of minimal area content connecting given boundaries.

Since the desired internal stress field is given, there is no material description needed and the problem reduces to a geometrical one even though the formulation is initiated by a mechanical equilibrium. Consequently, the input parameters required for the solution of the form finding problem without external loading is a set of Dirichlet boundary conditions on a boundary Γ and a stress field $\boldsymbol{\sigma}_0$ defined on the deformed geometry.

Again, optimal positions of the shape variables $\boldsymbol{s}$ have to be found. Typically, the tangential mesh related variables $\boldsymbol{r}$ cannot be eliminated to allow for large changes of shape. They remain as unknowns in the formulation. As a consequence, the resulting problem is singular with respect to the mesh related variables $\boldsymbol{r}$ because of the non-uniqueness of the discretization [19]. In particular, the reason is that the base vectors of $\boldsymbol{\sigma}_0$ are related to the unknown geometry and are functions of $\boldsymbol{r}$ as well. Also, the governing equations are non-linear in $\boldsymbol{s}$ and $\boldsymbol{r}$.

For the regularization of the problem, the Updated Reference Strategy is suggested [19]. In this method the problem is solved on the "updated reference geometry" of the form finding step (i):

$$\delta w(\boldsymbol{s},\boldsymbol{r}) = t\int_{A^i} \boldsymbol{S}^i : \delta\boldsymbol{E} dA^i = 0, \tag{9}$$

where $\boldsymbol{S}^i$ is the 2nd Piola–Kirchhoff stress tensor acting on the updated reference geometry and $\boldsymbol{E}$ the Green–Lagrange strain tensor. The updated reference geometry of step (i) with surface area A^i is defined as the intermediate equilibrium shape of the previous step $(i-1)$. If the stress tensor $\boldsymbol{S}^i$ was defined from a "pull back" operation of the Cauchy stress tensor $\boldsymbol{\sigma}_0$, Eq. (8) would remain unaltered as well as the singularity with respect to $\boldsymbol{r}$. Instead, $\boldsymbol{S}^i$ is defined by the equivalent components of $\boldsymbol{\sigma}_0$ with respect to the covariant base vectors $\boldsymbol{G}^i_\alpha$ of the updated reference geometry, defined later in the text, which remain fixed in the iteration step (i):

$$\boldsymbol{S}^i = \sigma_0^{\alpha\beta^i}\boldsymbol{G}^i_\alpha \otimes \boldsymbol{G}^i_\beta. \tag{10}$$

As a consequence, Eq. (9) is well defined and even linear with respect to $\boldsymbol{s}$ and $\boldsymbol{r}$ and both, the shape and the mesh are uniquely and smoothly modified during the form finding procedure [23]. As the updated reference reaches the final shape, the Cauchy stress defined in the actual configuration at iteration step (i), σ_0^i converges to σ_0.

Applying the method, the free-form shape of Fig. 1(b) is obtained for a predefined stress field $\boldsymbol{\sigma}_0$ and a set of Dirichlet boundary conditions. In this example, the four corner points are fixed and prestressed cables are supporting the edges of the membrane. Furthermore, since Eq. (9) is solved numerically, an initial discretization is required to initiate the procedure (Fig. 1(a)).

Neither the initial discretization nor the initial geometry influence the final shape obtained by form finding. However, the discretization describing the final shape is highly influenced by the initial one because of the update rule for the reference geometry. The initial mesh is the seed of the iteration sequence. For instance, by changing the initial discretization of the problem of Fig. 1 by adding a refinement (Fig. 2(a)) while keeping the same set of boundary conditions and prestress, solution of form finding will lead to the same shape, with the difference that the refinement of the initial mesh is maintained in the final one (Fig. 2). Consequently, the final mesh is influenced by, and closely related to the initial one, while the final shape obtained with the method is unique and independent of the initial geometry.

The same principle applies to the mesh regularization method, with the difference that this time the shape has to be retained and the discretization has to be improved. The point of departure is again Eq. (8). Now, a "template" or "ideal" element is defined as the reference configuration and the movement is restricted to the surface directions $\boldsymbol{r}$ since the surface geometry should remain unchanged. The template element describes the desired shape for each individual element and is described in detail in the next section. The shape is retained by applying additional Dirichlet boundary conditions normal to the surface for each surface node. In this work the multi-freedom constraints were implemented based on the master–slave method.

Applying these constraints and numerically solving the equilibrium, leads to a non-singular system of equations which is linear in the surface tangent space. As a consequence, the proposed method will generate proper meshes even for large distortions of the surface (or volumetric) mesh after solving one linear system of equations. Here, Eq. (9) is solved by the finite element method. For this, the discretization is done in the reference configuration as defined by the template using the isoparametric element concept [22], i.e. the surface geometry

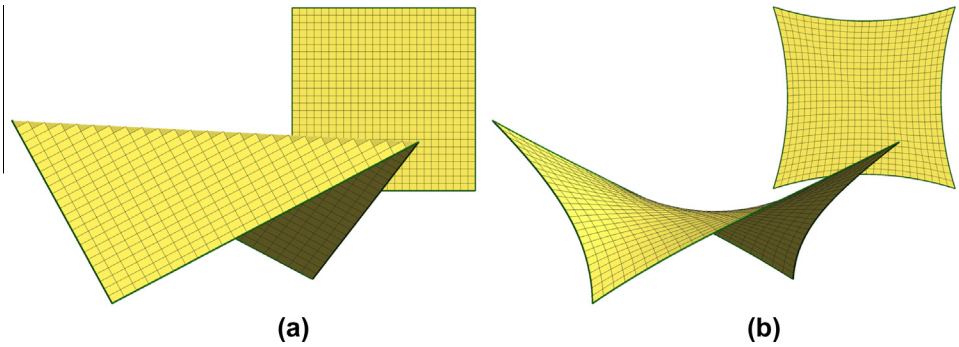

Fig. 1. Initial discretization (a) and final shape (b) after form finding of a 4-point membrane structure.

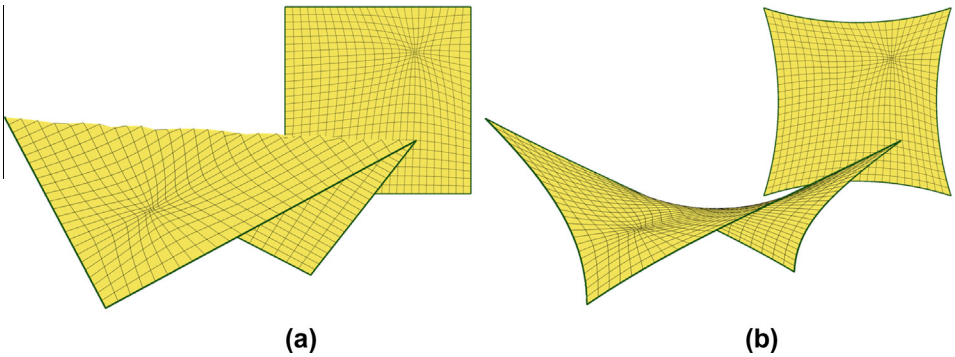

Fig. 2. Form finding of a 4-point membrane structure with local refinement on the initial mesh.

and the displacement field are piecewise approximated by the interpolation of nodal coordinates and displacements, respectively:

$$\boldsymbol{X} = \sum_{i=1}^{n} N^i(\theta^1, \theta^2)\boldsymbol{X}_i; \quad \boldsymbol{u} = \sum_{i=1}^{n} N^i(\theta^1, \theta^2)\boldsymbol{u}_i, \tag{11}$$

where N^i are the standard linear shape functions and n is the number of nodes (Fig. 3). The nodal displacements $\boldsymbol{u}_i,\ i = 1, \ldots, n$ are the unknowns of Eq. (9) and represent in this case the change of the mesh relevant tangential variable $\boldsymbol{r}$ and the amount that each node should displace in the tangential space in order to regularize the mesh. Consequently, the position of a surface point in the actual configuration is defined as:

$$\boldsymbol{x} = \sum_{i=1}^{n} N^i(\theta^1, \theta^2)(\boldsymbol{X}_i + \boldsymbol{u}_i). \tag{12}$$

In this context, the base vectors on the reference and on the actual configuration, respectively are:

$$\boldsymbol{G}_\alpha = \frac{\partial \boldsymbol{X}}{\partial \theta^\alpha} = \sum_{i=1}^{n} \frac{\partial N^i(\theta^1, \theta^2)}{\partial \theta^\alpha}\boldsymbol{X}_i; \quad \boldsymbol{g}_\alpha = \frac{\partial \boldsymbol{x}}{\partial \theta^\alpha} = \sum_{i=1}^{n} \frac{\partial N^i(\theta^1, \theta^2)}{\partial \theta^\alpha}\boldsymbol{x}_i, \quad \alpha = 1, 2. \tag{13}$$

On this basis, the 2nd Piola Kirchhoff stress and the Green–Lagrange strain are defined in the reference configuration accordingly:

$$\boldsymbol{S} = S^{\alpha\beta}\boldsymbol{G}_\alpha \otimes \boldsymbol{G}_\beta, \tag{14}$$

$$\boldsymbol{E} = E_{\alpha\beta}\boldsymbol{G}^\alpha \otimes \boldsymbol{G}^\beta = \frac{1}{2}(\boldsymbol{g}_\alpha \cdot \boldsymbol{g}_\beta - \boldsymbol{G}_\alpha \cdot \boldsymbol{G}_\beta)\boldsymbol{G}^\alpha \otimes \boldsymbol{G}^\beta, \quad \alpha, \beta = 1, 2. \tag{15}$$

Hence, taking the variation of Eq. (9) with respect to the unknown displacements $u_m, m = 0, \ldots, dofs$ and substituting Eq. (14) and Eq. (15) to Eq. (9), it can be rewritten for each degree of freedom m of the system as:

$$t\int_A \boldsymbol{S} : \frac{\partial \boldsymbol{E}}{\partial u_m} dA = t\int_A S^{\alpha\beta}\frac{1}{2}(\boldsymbol{g}_\alpha \cdot \boldsymbol{g}_{\beta,m} + \boldsymbol{g}_\beta \cdot \boldsymbol{g}_{\alpha,m})dA = 0, \quad m = 0, \ldots, ndofs. \tag{16}$$

This equation system with the displacements $\boldsymbol{u}_i$ as the unknowns is linear. The resulting stiffness matrix is:

$$K_{mn} = \int_A \boldsymbol{S} : \frac{\partial^2 \boldsymbol{E}}{\partial u_m \partial u_n} dA, \quad m, n = 0, \ldots, ndofs, \tag{17}$$

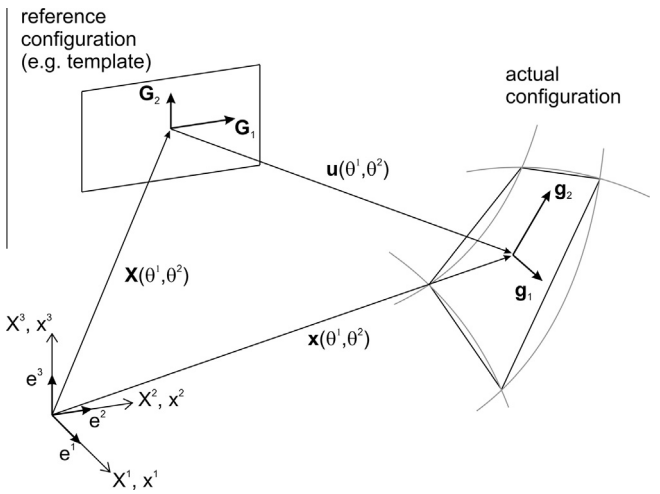

Fig. 3. Deformation in the context of geometrical nonlinear analysis.

whereas the right hand side is:

$$R_m = \int_A \boldsymbol{S} : \frac{\partial \boldsymbol{E}}{\partial u_m} dA, \quad m = 0, \ldots, ndofs. \tag{18}$$

The unknown of this system is the update of the displacement $\Delta \boldsymbol{u}_i$ and since the initial system is linear, the problem is solved in one step. In the case that the prescribed stress tensor is symmetric, the stiffness matrix and the right hand side reduce to:

$$\begin{aligned} K_{mn} &= \int_A S^{\alpha\beta} \cdot (\boldsymbol{g}_{\alpha,m} \cdot \boldsymbol{g}_{\beta,n}) dA, \\ R_m &= \int_A S^{\alpha\beta} \cdot (\boldsymbol{g}_{\alpha,m} \cdot \boldsymbol{g}_{\beta}) dA, \quad m, n = 0, \ldots, ndofs. \end{aligned} \tag{19}$$

In the above equations $S^{\alpha\beta}$ are the components of the predefined 2nd Piola–Kirchhoff stress tensor and $\boldsymbol{g}_{\alpha,m}, \alpha = 1, 2$ are the derivatives of the base vectors of the actual configuration with respect to the displacement of the mth degree of freedom. However, the integration is done in the reference configuration. In the reference configuration each element is assumed to have an ideal shape, i.e. its template. The individual templates are acting independently and there is no need that they match geometrically. For instance, as described also in the next section, the template can be a unit square for each element. Consequently, the calculation of the base vectors $\boldsymbol{G}_\alpha, \alpha = 1, 2$, the 2nd Piola–Kirchhoff stress tensor, the Green–Lagrange strain as well as the area A are evaluated based on this template element.

As it can be seen from Eq. (19) there is no dependency of the stiffness matrix to the unknown displacement field since the stiffness matrix depends only on the constant predefined 2nd Piola–Kirchhoff stress tensor $\boldsymbol{S}$ and on the derivatives of the base vectors with respect to the displacements which are constant values as well. Thus, the problem of in-plane regularization is linear.

As it was discussed earlier, when the method is applied to three-dimensional surfaces, additional Dirichlet boundary conditions have to be enforced in order to retain the shape. In practice, each node is restricted to move in the tangential plane to the surface at that point. The tangential plane is calculated by a weighted averaging of the normals of all the elements sharing the node. Here, each normal is weighted by the inverse of the element area. This averaging results in a more accurate normal direction compared to equally weighted averaging. For instance in a 2D case, the average of the weighted normals of each element around a node points exactly to the center of a circle passing through the discretization points. Of course, this is only an approximation and since the movement of each node during the process is finite, the nodes will deviate from the original surface. However, the true surface is usually not analytically given. These deviations are automatically corrected during shape optimization when the shape in normal direction is simultaneously modified. Moreover, if needed, higher order local approximations of the surface can also be used which of course will damage the linearity of the problem. In case of corners and sharp edges the nodes are fixed since these areas should be regarded as features of the initial design which should be retained during regularization.

Furthermore, in the special case of a square initial template for all the surface elements and an isotropic stress state, the problem reduces to the linear Amsden–Hirt method described earlier. One can easily conclude this statement by comparing the variational form of the Amsden–Hirt generator given in Eq. (20) and the variational form of the in-plane regularization problem:

$$U = t \int_A \boldsymbol{S} : \boldsymbol{E} dA. \tag{20}$$

Hence, the method can be regarded as a generalization of the Amsden–Hirt method which offers two additional mesh control parameters: the ideal (target) element shape which can be individually assigned for each element and the prestress controlling the size or concentration of the elements. These control parameters are discussed in detail in the following section.

5. The template element

The kernel of the in-plane regularization method is the proper choice of adequate element reference geometries or "element templates" and the choice of the applied prestress. These are the two handles used during

optimization to control the mesh. The template is the ideal shape of each element defined in the reference configuration. Obviously, for a given surface discretization there will not be any modification if the actual element geometries are taken as templates assuming a unit stress tensor. In any other case, each element will change its shape towards its template shape in a global sense.

The use of different templates and the role of the predefined stress field $\boldsymbol{S}$ can be demonstrated with the 9-element example of Fig. 4. In this example the nodes are placed in an irregular distance from each other. Keeping the geometry of the boundaries by applying proper boundary conditions and applying in-plane regularization using square templates and a unit stress field will lead to the second figure from the top of Fig. 4. Here, the shape of the elements changes in order to approach the square template in a global sense, conforming the Dirichlet boundary conditions. Since during this process no element is preferred, the elements cover the same distances over the span of the geometry and the skewness is automatically corrected.

Changing the applied stress field changes the relative size of elements. In the third figure from top of Fig. 4, elements 4 and 3 have three and two times more stress, respectively than the rest of the elements. As a result, these elements will cover three and two times less distance in the spanwise direction of the domain respectively. In general, higher predefined stress will cause elements to shrink which is a property which can be applied to achieve local refinements on the boundary or even inside the computational domain.

A more local effect is observed by using a rectangular template with edges as large as the midsegment of each element. This individual template for each element corrects the skewness locally (Fig. 4). Obviously, stress adaptation in desired areas can also be achieved.

In evolutionary problems, like in shape optimization or problems with moving boundaries, the goal is to retain the quality of the initial mesh which usually possesses certain properties like local refinements, boundary confined element layers and certain growth ratios between the elements. In this type of problems the initial shape of each element is regarded as the template and throughout the evolution of the process the elements retain their shape and size independent of the number of steps required to arrive at the specific deformed state. For instance, by moving the right boundary of the initial example of Fig. 4 together with this type of template results to the bottom mesh of Fig. 4. It is obvious that after the deformation the elements keep their initial properties.

The method applies correspondingly to more dimensions. For instance, in Fig. 5(a) a square template and a unit stress tensor is applied as reference geometry to remove the distortion (noise) from a two-dimensional

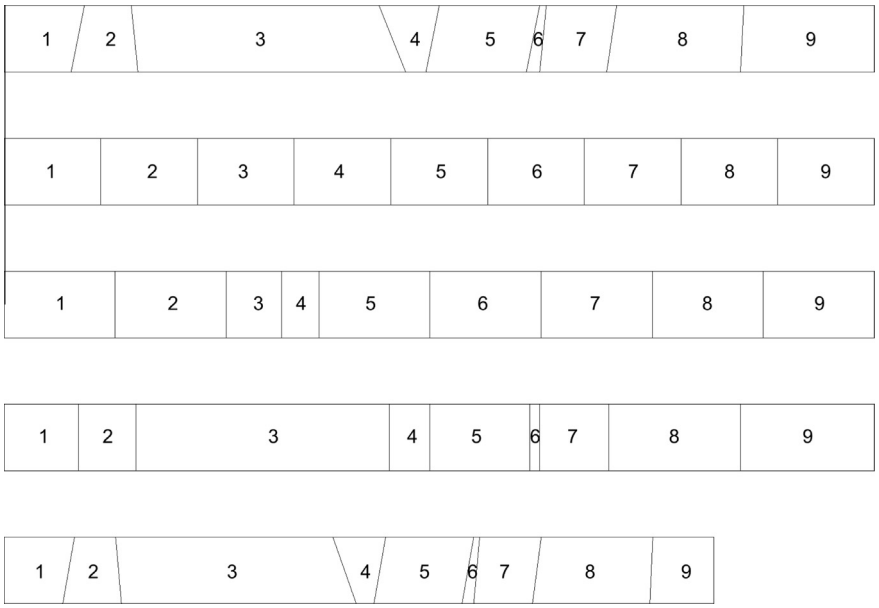

Fig. 4. Demonstration of the in-plane regularization method for a simple 9-element example. From top to bottom: initial mesh, regularization with square templates, regularization with square templates with local refinement, regularization with shearless templates, regularization with initial templates in a moving boundary problem.

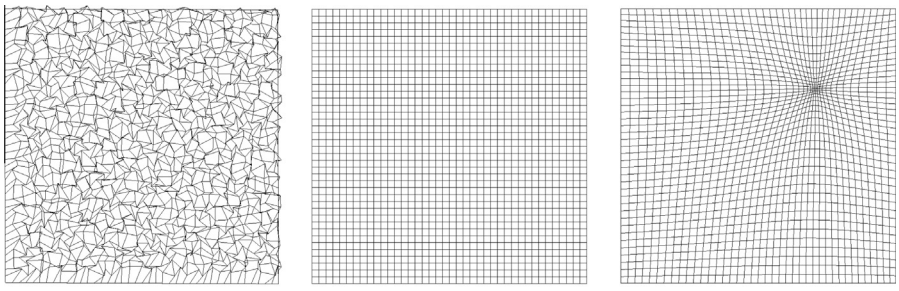

Fig. 5. Noise removal and local refinement around a point.

plane mesh consisting of quad elements. Fig. 5(b) shows the mesh after regularization, i.e. the solution of a linear system of equations. The same square template was used for every element and the resulting mesh consists of elements which match perfectly the predefined template. In this particular case the topology of the mesh allows the elements to reach their template shape. In general, this is not the case and thus the method results in a global compromise after this linear step. As it has been already shown for the one-dimensional case, changing the applied local prestress, local refinements can be achieved. In Fig. 5(c), the isotropic stress decrease when the distance to the refinement point increases.

In the same way, proper refinement needed for boundary layer resolution in fluid problems can be achieved with one linear step starting from any initial mesh. Moreover, as in the one-dimensional case, by assuming for each element, a rectangular template with edges as large as the midsegment of each element, the skewness of elements can be reduced. In the next example, the mesh of Fig. 6(a) created by a mesh generator will be improved using this template. The elements of this mesh are not severely distorted as in the previous example but still there is a group of elements around the boundary circle which are not well aligned to the boundary. This type of non orthogonality is a remarkable source of error in numerical simulations, especially in the finite volume method. In the resulting mesh shown in Fig. 6(b), the first layers of elements around the circle are following the curved lines of the boundary. In Fig. 7 the distribution of the angle of distortion is plotted. Here,

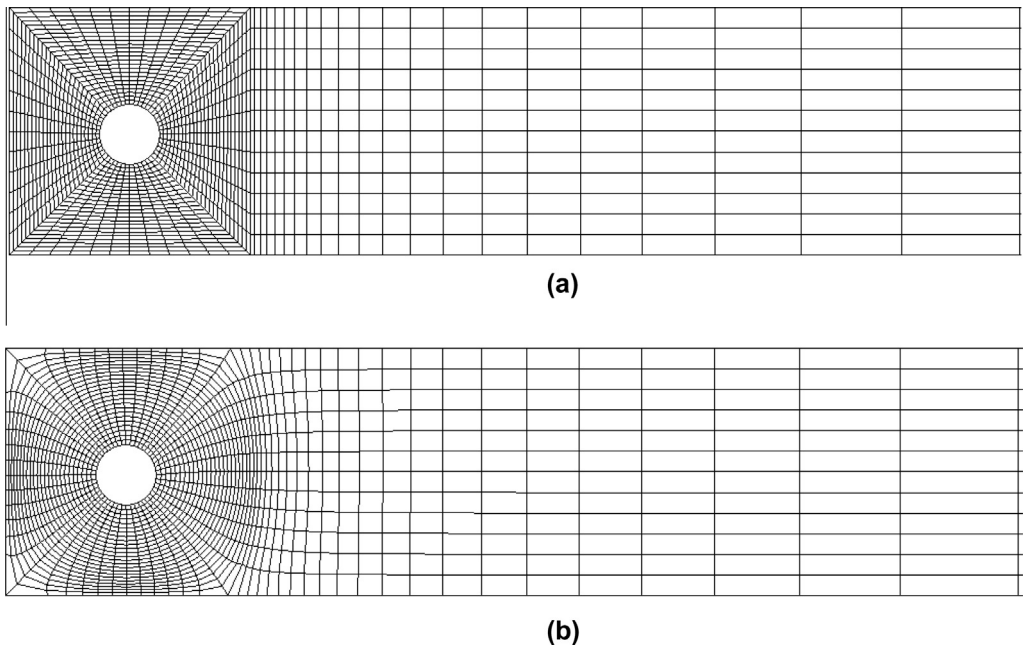

Fig. 6. Regularization of a structured mesh with a hole.

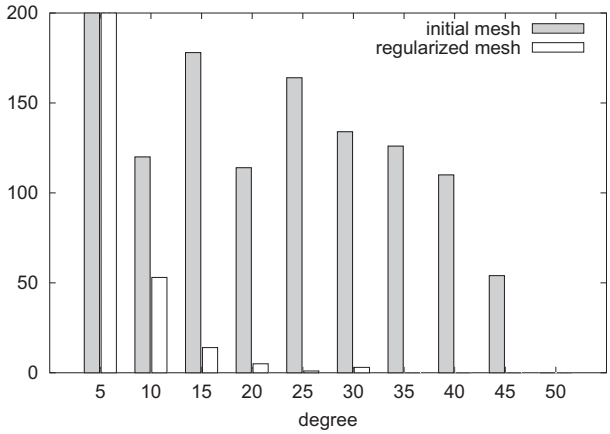

Fig. 7. Distribution of angle of distortion in initial and regularized mesh.

the angle of distortion is defined as $|90 - \phi|$, where ϕ is the angle between the midsegments of the quadrilateral. It can be observed that the mesh quality is significantly improved after regularization while more elements have small distortion angles and the elements with bigger distortion angles are less. The method can not guarantee non-folded grids when used for mesh smoothing like in this example but in many cases it can be used to improve the quality of the mesh with a proper choice of individual templates. For problems with sharp reentrant corners like the ones presented in the Rouge's Gallery [11], nonlinear procedures are required and the reader can refer to [13].

These limitations do not apply in the case of evolutionary processes which begin with an initial high quality mesh which gets distorted during the computation. For this type of problems, the initial shape of each element can be used as the template as described for the one-dimensional case. Examples of such problems are CFD simulations with moving boundaries or fluid–structure interaction problems.

As commonly observed in engineering practice, the increase in the curvature of the surface mesh can have severe effects on the mesh quality. In Fig. 8(a), the resulting mesh of an initially flat surface, after applying a displacement field normal to the surface in 100 iterations is shown. This can be the case, for example, in a metal forming process or the inflation of a rubber membrane as anticipated in figure (Fig. 8). The resulting elements are elongated, even though, the initial mesh had a good quality consisting of square elements of the same size. Applying the regularization method together with the initial shape of each element as template, the elements of the deformed shape still have very good aspect ratios (Fig. 8(b)). Moreover, since this method regularizes the mesh globally, there are no more elements with high aspect ratios, for the price that some of the elements with perfect initial aspect ratios were slightly deformed (Fig. 9). This is exactly what is desired in shape optimization, because the low quality elements are the ones which limit the computation. The

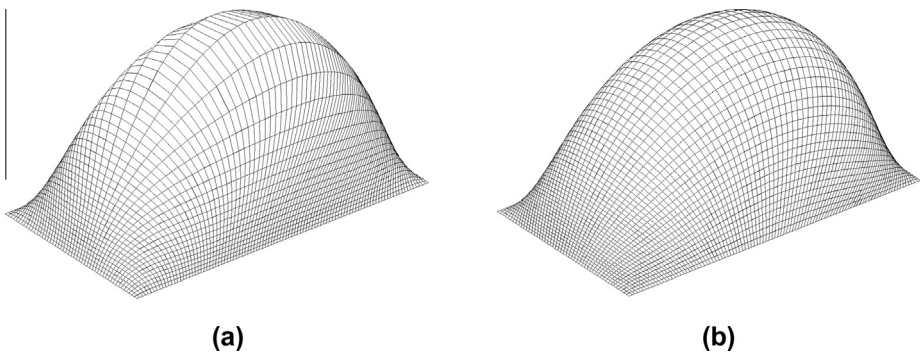

Fig. 8. The resulting mesh after a curving process without and with regularization, respectively.

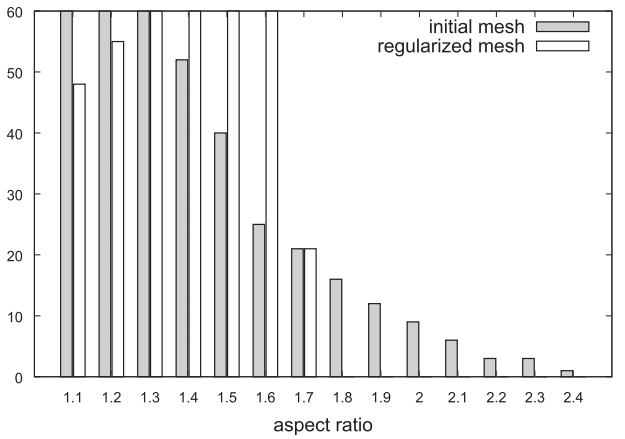

Fig. 9. Distribution of element aspect ratio (ratio of midsegments) on final design with and without regularization.

transmission from a flat or slightly curved surface to highly curved one is a common incident in node-based optimization as well.

From all the above, it follows that the choice of the template and the prestress is decisive for each application. For optimization problems the most suitable template is the one with the initial shape of each element.

6. Minimization of power dissipation in an S-bend 3D duct

In this section the in-plane regularization method is successfully applied to the shape optimization of a three-dimensional industrial S-bend (Fig. 10). The air duct used for rear seat ventilation is studied in [24]. The design surface is depicted with green in Fig. 10 and has 8324 nodes and thus design variables $\boldsymbol{s}$.

The objective function is the dissipated power defined in [25]:

$$f = -\int_{\Gamma}\left(p+\frac{1}{2}\rho\boldsymbol{v}^2\right)\boldsymbol{v}\cdot\boldsymbol{n}d\Gamma, \tag{21}$$

where p and $\boldsymbol{v}$ are the pressure and the velocity, respectively whereas $\boldsymbol{v}\cdot\boldsymbol{n}$ is the normal component of the velocity and Γ the fluid boundary.

Furthermore, for the shape optimization the node-based approach is applied where the design variables of the problem are the components perpendicular to the surface at each node and the optimization algorithm is steepest descent with constant step size. In this case, for the sensitivity analysis, a continuous adjoint method [25,26] was applied due to its significant advantages over the direct sensitivity analysis [27], using OpenFOAM. The resulting sensitivity field is not smooth and an explicit Gaussian filtering is performed. After the

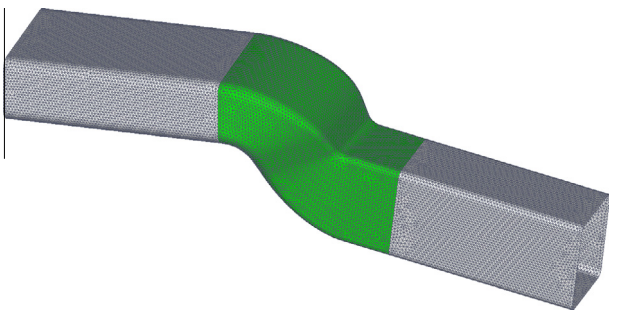

Fig. 10. Initial mesh of S-bend with 2081346 finite volume cells. The design surface is marked with green [24]. (For interpretation of the references to colour in this figure caption, the reader is referred to the web version of this article.)

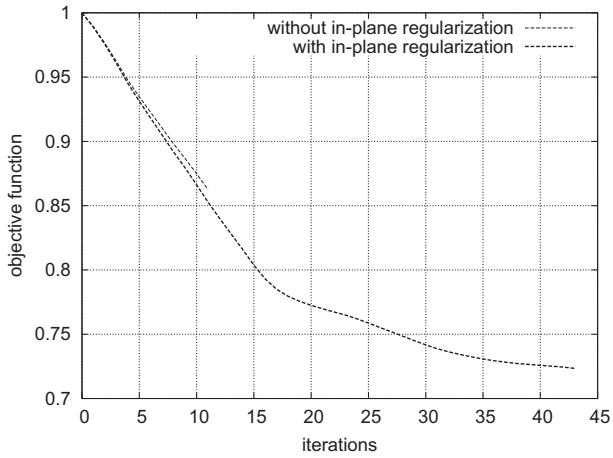

Fig. 11. Histories for the normalized power dissipation with and without in-plane regularization.

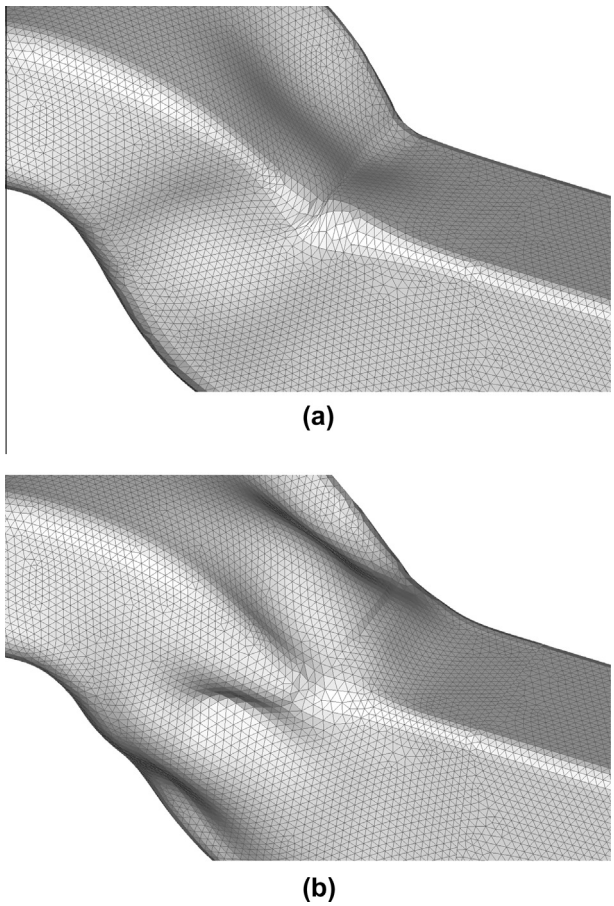

Fig. 12. Shape optimization of S-bend. Failure of the mesh at the 11th iteration without in-plane regularization (a) and final design (43rd iteration) with in-plane regularization with 27% of improvement of the objective (b).

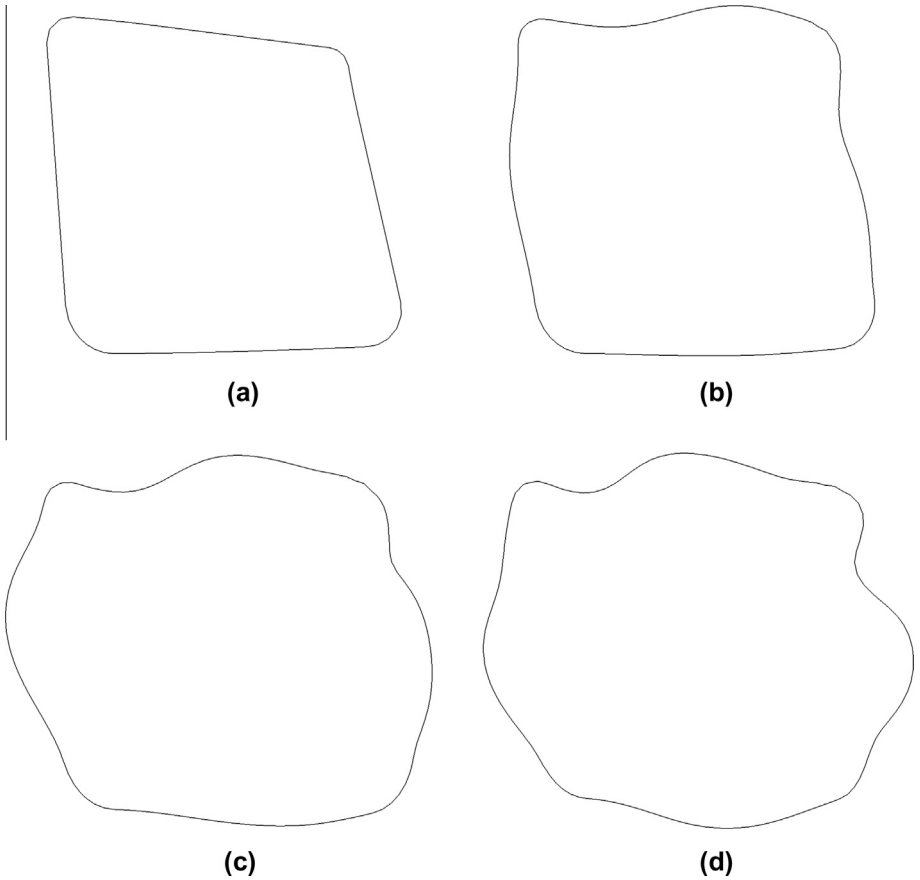

Fig. 13. Cross sections at the bend for iterations 11, 22, 33 and 43, respectively.

optimization update, the in-plane regularization method is applied to improve the quality of the mesh. At the end of each optimization step the volume mesh is updated by solving the Laplacian equation with variable diffusion [14].

By applying out-plane and in-plane regularization as already described above, around 27% of improvement in power loss is achieved (Fig. 11). In this way significant design changes can take place while no kinks, wrinkles or any other mesh irregularities appear throughout the computation. The final design is smooth and the mesh density and quality is maintained (Fig. 12(b)). The evolution of the shape at a cross section located at the bend of the duct is shown in Fig. 13. In contrary, without in-plane regularization the optimization fails already at the 11th iteration due to degenerated elements which appear on the bend of the duct as it can be seen in Fig. 12(a). Fig. 14 displays the surface sensitivity at the initial design as well as at the improved design using in-plane regularization. The high sensitivity region undergoes the largest deformation. This area is where the mesh fails when no in-plane regularization is applied. In the final design the high sensitivities are removed while some sensitivity still remains close to the boundary of the design domain since it should be kept unchanged during optimization.

In order to study the mesh quality more quantitatively, the proportional change of area of the surface elements compared to the initial mesh is shown in Fig. 15. The value 0 means that the area of the element has not been changed and the value -1 shows an element with zero area. Note that Fig. 15(b) refers to iteration 43 and Fig. 15(a) to iteration 11, at which the case with no in-plane treatment collapses. Although the shape is much more deformed in 15(b), the elements still have much better quality compared to 15(a).

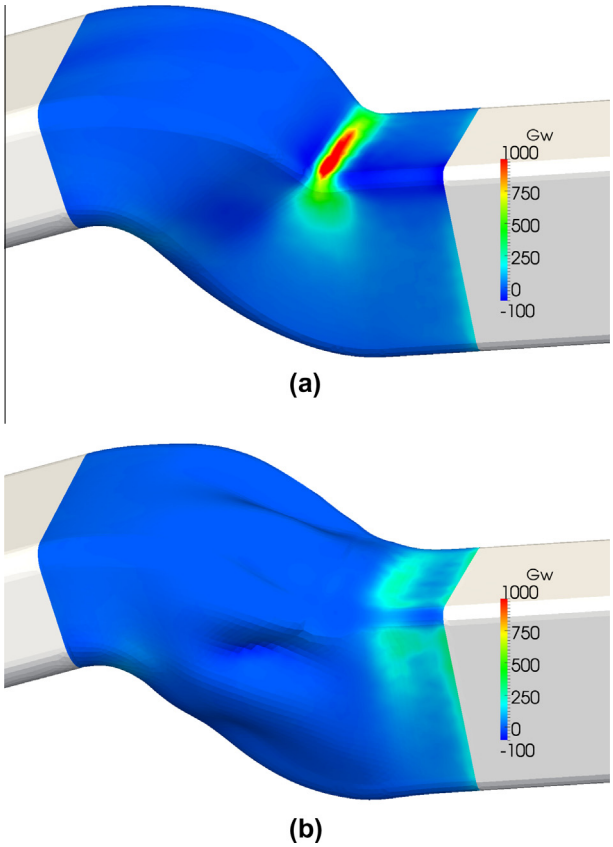

Fig. 14. Surface sensitivity distribution for the initial and final design.

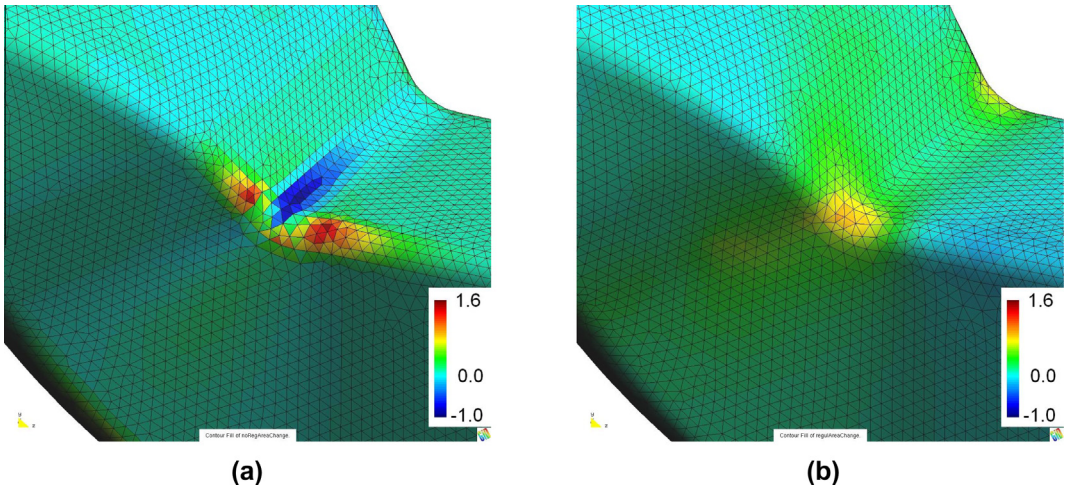

Fig. 15. Proportional change of element area w.r.t the initial mesh without (a) and with (b) in-plane regularization, plotted on the initial shape.

7. Conclusions

In this work, an in-plane regularization method is proposed to retain the quality of surface meshes during node-based shape optimization. The method is an elliptic method motivated by form finding: A numerical

method to determine the shape of prestressed membrane structures. Important parameters of the method are the reference or "template" element and the "artificial" prestress, both of which are defined for each individual element. On the one hand, the template controls the final shape of each element: each element approaches its template as close as possible in a global sense. On the other hand, the stress influences the relative size of each element compared to the rest. Depending on these two parameters, in-plane regularization can be applied for mesh smoothing, mesh motion and local refinement. The method is tested by various examples and as it is shown in the final ducted flow example, the in-plane treatment is necessary for keeping mesh quality and achieving considerable reduction of the objective function values.

Acknowledgments

The authors acknowledge support by the European Commission under THEME SST.2007-RTD-1: Competitive product development, as part of the project FLOWHEAD (Fluid Optimisation Workflows for Highly Effective Automotive Development Processes), from February 2009 to January 2012.

References

[1] A. Jameson, L. Martinelli, N. Pierce, Optimum aerodynamic design using the Navier–Stokes equations, Theor. Comput. Fluid Dyn. 10 (1998) 213–237.
[2] O. Soto, R. Löhner, Cfd shape optimization using an incomplete-gradient adjoint formulation, Int. J. Numer. Methods Eng. 51 (2001) 735–753.
[3] B. Mohammadi, O. Pironneau, Applied Shape Optimization for Fluids, Numerical Mathematics and Scientific Computation, Oxford University Press, 2009.
[4] B. Mohammadi, Shape optimization for 3d turbulent flows using automatic differentiation, Int. J. Comput. Fluid Dyn. 11 (1998) 27–50.
[5] C. Le, T. Bruns, D. Tortorelli, A gradient-based, parameter-free approach to shape optimization, Comput. Methods Appl. Mech. Eng. 200 (2011) 985–996.
[6] A. Stück, T. Rung, Adjoint rans with filtered shape derivatives for hydrodynamic optimisation, Comput. Fluids 47 (2011) 22–32.
[7] M. Hojjat, E. Stavropoulou, K.-U. Bletzinger, The vertex morphing method for node-based shape optimization, Comput. Methods Appl. Mech. Eng. (2013).
[8] M. Scherer, R. Denzer, P. Steinmann, A fictitious energy approach for shape optimization, Int. J. Numer. Methods Eng. 82 (2010) 269–302.
[9] X. Jiao, Face offsetting: a unified approach for explicit moving interfaces, J. Comput. Phys. 220 (2007) 612–625.
[10] J. Thompson, B. Soni, N. Weatherill, Handbook of Grid Generation, CRC Press, 1999.
[11] P. Knupp, S. Steinberg, The Fundamentals of Grid Generation, CRC Press, 1993.
[12] A. Winslow, Numerical solution of the quasilinear poisson equation in a nonuniform triangle mesh, J. Comput. Phys. 1 (1966) 149–172.
[13] G. Hansen, R. Douglass, A. Zardecki, Mesh Enhancement: Selected Elliptic Methods, Foundations and Applications, Imperial College Press, 2005.
[14] H. Jasak, Z. Tukovic, Automatic mesh motion for the unstructured finite volume method, Trans. FAMENA 30 (2006) 1–20.
[15] A. De Boer, M. Van der Schoot, H. Bijl, Mesh deformation based on radial basis function interpolation, Comput. Struct. 85 (2007) 784–795.
[16] C. Degand, C. Farhat, A three-dimensional torsional spring analogy method for unstructured dynamic meshes, Comput. Struct. 80 (2002) 305–316.
[17] P. Knupp, Winslow smoothing on two-dimensional unstructured meshes, Eng. Comput. 15 (1999) 263–268.
[18] G. Hansen, A. Zardecki, D. Greening, R. Bos, A finite element method for unstructured grid smoothing, J. Comput. Phys. 194 (2004) 611–631.
[19] K. Bletzinger, E. Ramm, A general finite element approach to the form finding of tensile structures by the updated reference strategy, Int. J. Space Struct. 14 (1999) 131–145.
[20] J. Linhard, K. Bletzinger, Tracing the equilibrium – recent advances in numerical form finding, Int. J. Space Struct. 25 (2010) 107–116.
[21] R. Wüchner, K. Bletzinger, Stress-adapted numerical form finding of pre-stressed surfaces by the updated reference strategy, Int. J. Numer. Methods Eng. 64 (2005) 143–166.
[22] J. Bonet, R. Wood, Nonlinear Continuum Mechanics for Finite Element Analysis, Cambridge Univ. Pr., 1997.
[23] K. Bletzinger, Form finding and optimization of membranes and minimal surfaces, Mitteilungen, Institut für Baustatik, 1998.
[24] C. Othmer, T. Kaminski, R. Giering, Computation of topological sensitivities in uid dynamics: cost function versatility, in: Proceedings of the European Conference on Computational Fluid Dynamics ECCOMAS CFD, Egmond aan Zee, Netherlands, 2006.
[25] C. Othmer, A continuous adjoint formulation for the computation of topological and surface sensitivities of ducted flows, Int. J. Numer. Methods Fluids 58 (2008) 861–877.

[26] D. Papadimitriou, K. Giannakoglou, A continuous adjoint method with objective function derivatives based on boundary integrals, for inviscid and viscous flows, Comput. Fluids 36 (2007) 325–341.
[27] A. Jameson, Optimum aerodynamic design using cfd and control theory, AIAA paper, 1729, 1995, pp. 124–131.